Journal of Nuclear Materials 492 (2017) 231–238

Contents lists available at ScienceDirect

Journal of Nuclear Materials

journal homepage: www.elsevier.com/locate/jnucmat

Americium and trivalent Lanthanides incorporation in high-level waste glass-ceramics

Isabelle Bardez-Giboire [a, *], Abdessamad Kidari [a], Magali Magnin [b], Jean-Luc Dussossoy [b], Sylvain Peuget [b], Richard Caraballo [b], Magaly Tribet [b], Franck Doreau [b], Christophe Jégou [b]

[a] CEA, DEN, DE2D, SEVT, Laboratoire d'études de Développement des Matrices de Conditionnement, F-30207 Bagnols-sur-Cèze, France
[b] CEA, DEN, DE2D, SEVT, Laboratoire d'étude des Matériaux et Procédés Actifs, F-30207 Bagnols-sur-Cèze, France

HIGHLIGHTS

- Actinides and Lanthanides behaviors are compared in glass and in a apatite ceramic phase.
- Composition, shape and cell parameters of Ln/Am apatite crystals are very close.
- Microstructures of Ln/Am glass-ceramics are very close.
- Structures of Ln/Am glassy phases are very close.

GRAPHICAL ABSTRACT

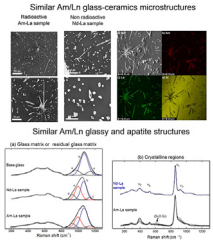

ARTICLE INFO

Article history:
Received 24 April 2017
Received in revised form
29 May 2017
Accepted 29 May 2017
Available online 30 May 2017

Keywords:
Glass-ceramic
Actinide
Lanthanide
High-level waste conditioning
Apatite

ABSTRACT

The incorporation and partitioning of americium and trivalent lanthanides were investigated in aluminoborosilicate glass-ceramics with apatite-like silicate crystals of general formula $Ca_2(Ln,Am)_8(SiO_4)_6O_2$.

A microstructural and structural study of two glass-ceramics containing Am_2O_3 - La_2O_3 or Nd_2O_3 - La_2O_3, respectively, was carried out by XRD, SEM/EDS and EMPA so as to assess a comparison of Lanthanides and Actinides partitioning into apatite crystals and residual glass. Moreover, Raman analyses of residual glasses were performed to compare the role of Am and Nd on the glassy structure.

Results put forward that shape, composition, Ln/Am stoichiometry and cell parameters of apatite crystals of both (Am-La) and (Nd-La) glass-ceramics are very close. This paper thus shows similar results for (Am-La) and (Nd-La) glass-ceramics in terms of apatite/glass partitioning and in terms of structural role on glassy structure. It can be therefore put forward that Nd^{3+} and Am^{3+} behaviors are close, either in the glass or in the crystalline structure.

1. Introduction

The conditioning of high level wastes coming from spent nuclear fuel reprocessing aims at stabilizing the radionuclides for geological time scale in bulk matrices. The compositions of these matrices must ensure good chemical durability, thermal and radiation stability in geological repositories. Current and past investigations have mainly considered amorphous and crystalline materials for the immobilization of specific wastes type or composition [1–8]. The industrial immobilization of radioactive wastes is in operation in several countries, each relying on specific technological solutions. This is the case for the French R7/T7 borosilicate glass which incorporates up to18.5 wt.% of high level wastes coming from reprocessed spent nuclear fuel [9].

Glass-ceramic matrices could be an alternative way to confine

* Corresponding author.
E-mail address: isabelle.giboire@cea.fr (I. Bardez-Giboire).

http://dx.doi.org/10.1016/j.jnucmat.2017.05.045
0022-3115/

high amounts of high level waste and could offer flexibility in the management of waste streams to be vitrified. Their design and development need to evaluate the partitioning of radionuclides into glassy and crystalline phases and also to master the crystallization phenomena.

Furthermore, the aspects of minor-actinides and lanthanides incorporation in glass and glass-ceramic matrices are of utmost interest, not only for the design of high level waste matrices but also for further understanding of the chemistry of minor-actinide elements. In a previous study, we have thoroughly investigated Lanthanides (Nd^{3+}, La^{3+}) incorporation and local environment in an aluminoborosilicate glassy system ($SiO_2 - B_2O_3 - Na_2O - Al_2O_3 - CaO - Nd_2O_3 - La_2O_3$) [10]. The changes in glass composition affect their local environment and their impact on the crystallization mechanisms [10–12]. Beyond the solubility limit, lanthanides elements are reported to form apatite phases with the general formula $Ca_2Ln_8(SiO_4)_6O_2$. It appeared that Ln_2O_3 solubility is higher for La-rich formulations than for Nd-rich ones and that an increase in the RE oxide content reduces the connectivity of the network building units through formation of non-bridging oxygens at the expense of the oxygen bridges. This depolymerization of the glass network did not affect neodymium environment which always consisted in silicate tetrahedra. The composition of the apatite crystals was found to be affected by the La and Nd contents of the parent glass and deviation from the ideal composition ($Ca_2Ln_8(SiO_4)_6O_2$) occurred in the neodymium end of the system (La/(La + Nd) ratio approaching zero). It thus appears that both Ln_2O_3 solubility and crystal composition are strongly dependent on the type and crystal chemistry of the Ln elements.

However, similar studies conducted with transuranic elements at concentrations exceeding their solubility or with glass-ceramic materials are limited. In glasses, even if introduced as Am^{4+} in AmO_2, americium stabilizes as Am^{3+} in borosilicate and aluminoborosilicate glasses [13,14]. Under this oxidation state (+III), Am^{3+} has a ionic radius of 0.097 nm and 0.108 nm when coordinated to 6 (CN6) and 8 (CN8) oxygen atoms, respectively [15]. These values are comparable to that of Nd^{3+}: 0.098 nm (CN6) and 0.111 nm (CN8) [16]. Moreover in crystalline structures, both elements are accommodated in their + III oxidation state: neodymium in apatite structures for example, [17] and americium in $AmNbTiO_6$ [17] and $AmPO_4$ [2,18].

To our knowledge, there are no previous reports of americium behavior in crystalline structures similar to those of the present study, the closest cases being that of $Ca_2Nd_8(SiO_4)_6O_2$ apatites containing ^{244}Cm formed in supercalcine ceramics [19] and that of $Ca_3Gd_7(SiO_4)_5(PO_4)O_2$ apatites like crystals containing ^{244}Cm formed in partially devitrified PNL 77-260 waste glass [20]. Nevertheless, none of these studies adressed the specific role and partitioning of Am in the glass-ceramic systems. In this paper, Lanthanides (Nd^{3+}, La^{3+}) and Actinides (Am^{3+}) incorporation and local environment were investigated in glass-ceramics of the $SiO_2 - B_2O_3 - Na_2O - Al_2O_3 - CaO - Ln_2O_3/Am_2O_3$ system (with Ln = Nd, La) for which the cumulative Ln_2O_3 - Am_2O_3 solubility limit was voluntarily exceeded, leading to the formation of apatite-like silicate crystals of general formula $Ca_2(Ln,Am)_8(SiO_4)_6O_2$. A comparison of Lanthanides and Am (particularly Nd and Am) partitioning into apatite crystals and residual glass was performed, focusing on the stoichiometry and cell parameters of Ln-apatite and Am-apatite crystals. Neodymium is generally considered as a good minor-actinide surrogate since both elements have similar ionic radii and identical oxidation states in the glass network and crystalline structures. However this was never experimentally confirmed. Therefore to this aim, two glass-ceramics (Am-La) and (Nd-La), respectively containing Am_2O_3 - La_2O_3 and Nd_2O_3 - La_2O_3, for which americium was fully substituted by neodymium on a molar basis, were elaborated and characterized. Structural and microstructural aspects were assessed by means of chemical analyses, spectroscopic and X-ray diffraction techniques. The relevant differences in the structure and composition of the amorphous and crystalline phases are reported, while the overall effects of replacing Am by Nd are discussed in light of the trivalent cations partitioning in the crystals and in the amorphous glassy matrix. These results provide valuable information on the partitioning of Am/Nd in the residual glass and on the Am-apatite chemistry above the $Ln_2O_3 - Am_2O_3$ solubility limit.

2. Materials and methods

2.1. Material fabrication

Two glass-ceramics (GC) called (Am-La) GC and (Nd-La) GC, respectively containing Am_2O_3 - La_2O_3 and Nd_2O_3 - La_2O_3, with a R ratio of 0.5 (R = La/(La + Am) or La/(La + Nd) [10]), were prepared in the $SiO_2 - B_2O_3 - Na_2O - Al_2O_3 - CaO - Ln_2O_3/Ac_2O_3$ system. Moreover a base glass SiO_2-B_2O_3-Na_2O-Al_2O_3-CaO was prepared as a structural reference without Nd and Am for comparing both role of Nd and Am by Raman spectroscopy analyses (Table 1).

Reagent grade SiO_2 (Millisil), H_3BO_3, Al_2O_3, Na_2CO_3, La_2O_3, Nd_2O_3 (Prolabo) and CaO (Alfa Aesar) were used along with americium oxide powder (AmO_2, Camix 85% ± 1 Am per g) with an isotopic composition of 99.99% ± 0.02 ^{241}Am.

Preparation and characterization operations of (Am-La) GC were conducted in dedicated hot cells of DHA laboratory located within ATALANTE facility. Under these conditions, it is possible to proceed with remote preparation and analysis of glasses with significant fractions of radionuclides. Prior to synthesis, the homogeneity of compositions with increasing lanthanides content (Nd_2O_3+La_2O_3 = 2.08, 2.66, 3.26, 3.90, 4.56 mol.% at La/(La + Nd) = 0.5) was assessed in a non-radioactive laboratory using an exact replica of the hot cell process. The solubility limit of Ln^{3+} elements (which corresponds to the last content before the appearance of apatite-like crystals $Ca_2Nd_xLa_{8-x}(SiO_4)_6O_2$ as seen in the previous study [10]) was established to be located between 2.66 and 3.26 mol.%. According to these results, the radioactive sample was batched with a La_2O_3+Am_2O_3 content of 3.90 mol.% with a ratio of La/(La + Am) = 0.5 so as to yield to a heterogeneous material (i) with sufficient crystallinity for convenient structural analyses and (ii) using realistic quantities of ^{241}Am (Table 1).

The hot cell sample preparation procedure used 5 g batch of glass-ceramic. Powders were first introduced in cylindrical Pt crucible (Ø 14.8 mm × 100 mm) in which 4 ml of deionized H_2O were added, followed by AmO_2 powder. The slurry was homogenized by means of an ultrasonic probe for several minutes. After homogenization, the Pt-crucible was placed in an alumina container, loaded in a graphite resistor furnace. The furnace atmosphere was then flushed with argon for 4 h. Melting took place at 1200 °C for 5.5 h (heating rate of around 50 °C.h^{-1} from room temperature to 800 °C then 100 °C.h^{-1} from 800 °C to 1200 °C). The melt was then cooled down to room temperature at 350 °C.h^{-1}.

To assess a pertinent comparison of Am and Nd behavior, preparation of (Nd-La) GC was performed under identical experimental conditions (reactant mixing and thermal treatments).

Furthermore, the fabrication of the base glass was done according a fabrication process described elsewhere [10].

2.2. Characterization

The ^{241}Am content of the (Am-La) sample was determined from the thermal output of the sample measured in a SETARAM C80D calorimeter (SETARAM, France) with a resolution of 1.2 × 10^{-7} W

Table 1
Molar compositions of (Am-La) and (Nd-La) glass-ceramics and Base glass.

	Composition in mol.%								R
	SiO_2	B_2O_3	Na_2O	Al_2O_3	CaO	La_2O_3	Am_2O_3	Nd_2O_3	
Am-La sample theoretical	56.60	10.19	16.12	4.99	8.21	1.95	1.95	—	0.50
Am-La sample corrected[a]	56.77	10.23	16.16	5.01	8.23	1.95	1.65	—	0.54
Nd-La sample	56.60	10.20	16.12	4.99	8.20	1.95	—	1.95	0.50
Base glass	58.89	10.61	16.77	5.19	8.51	—	—	—	

R = La/(La + Am) or La/(La + Nd).
[a] Corrected to the Am content measured by Calorimetry.

and a detection limit of 2×10^{-6} W. The average of three measurements was converted into Am_2O_3 considering a decay heat of 0.11 W/g of ^{241}Am.

Following analysis of the americium content, the initial cylindrical (Am-La) sample was cut in two parts and both samples were embedded in a Wood's alloy or epoxy resin and furthermore polished for subsequent structural and microstructural investigations.

X-ray diffraction patterns were recorded using a Seifert 3000 diffractometer (GE Sensing, France) equipped with a Mo source ($\lambda = 0.07093$ nm) (40 kV, 30 mA) and on a Phillips X'pert PRO instrument (PANalytical, Netherlands) operated with a Cu source ($\lambda = 0.15406$ nm) (40 kV, 40 mA) for the active (Am-La) and non-active (Nd-La) samples, respectively. After extraction of the space groups, the profiles were fitted by the Le Bail method using the FULLPROF program [21].

Scanning electron micrographs were collected on carbon-coated samples with a JEOL 6300 (JEOL, Japan) scanning electron microscopes (SEM, 15 kV) and a Philips XL30 (Philips, Netherlands) for (Am-La) and (Nd-La) samples, respectively.

The chemical composition of the (Am-La) sample was determined by means of a CAMECA SX 50 electron probe micro analyzer (EMPA, Cameca, France) equipped with four X-ray spectrometers and TAP/PET crystals and operated under an acceleration voltage of 20 kV and 20 nA stabilized beam. The chemical composition of the (Nd-La) sample was determined by means of a CAMECA SX 100 electron probe micro analyzer (EMPA, Cameca, France) equipped with four X-ray spectrometers (LPC3, LTAP, LPET and PET crystals) and an acceleration voltage of 12 kV and 10 nA stabilized beam.

For (Am-La) glass-ceramic, Raman spectra were collected with a Horiba HR-800micro-spectrometer (Horiba, UK) using a 532 nm green laser source located outside the hot cell and coupled to an optical microscope with x1.25 to x100 objectives (Optic Peter, France) located within the hot cell. A grating of 1800 mm^{-1} and a slit size of 125 μm were used. For (Nd-La) sample, Raman spectra were also collected with a Horiba HR-800micro-spectrometer with a green laser at 532 nm. The beam was focused on the sample with x50 and x100 objectives (Olympus BX41) and the spectra collected between 200 and 1600 cm^{-1} (1800 mm^{-1} grating, 100 μm slit and 200 μm confocal hole). All the spectra were corrected for temperature and frequency dependent scattering intensity [22] and the baseline subtracted.

3. Results

3.1. Am content

After removal of the platinum crucible (Fig. 1-(a)), calorimetric analyses indicated an average thermal power output that corresponds to ~1.65 mol.% Am_2O_3 instead of the 1.95 mol.% theoretical value. Therefore the (Am-La) GC composition was recalculated, noted "(Am-La) GC corrected" in Table 1.

Then, the crude sample was embedded and polished (Fig. 1-(b)) for optical and electronic microscopic observations.

3.2. Microstructure

Optical microscopy images of the (Am-La) GC confirmed its glass-ceramic character under polarized light, with a homogeneous dispersion of the crystals within the sample (Fig. 1-(c-e)). The (Nd-La) GC synthesized under identical conditions showed similar features (Fig. 2-(a-b)).

Scanning electron microscopy (SEM) revealed hexagonal shaped crystals (white phase on the SEM micrographs) of varying sizes and orientations in both radioactive (Fig. 3(a–c)) and non-radioactive samples (Fig. 3(d–f)). In addition, back scattered electron imaging reveal a similar contrast between the amorphous and crystalline regions of the (Am-La) and (Nd-La) GCs, that could state for close compositions of the (Am-La) and (Nd-La) residual glassy phase on the one hand and (Am-La) and (Nd-La) crystalline ones on the other hand.

3.3. Structure and composition of crystalline and glassy phases

X-ray diffraction measurement of the (Am-La) GC (Fig. 4-(a)) showed reflections unequivocally corresponding to that of hexagonal apatite-like silicate structure ($P6_3/m$ space group) with the general formula $Ca_2RE_8(SiO_4)_6O_2$, where RE is a trivalent cation. The same crystalline structure was identified in the (Nd-La) GC (Fig. 4-(b)). The refinement of the lattice parameters indicates that cell parameters of crystal phases formed in (Am-La) and (Nd-La) GCs are very close ($a_{Am\text{-}La} = 0.960$ nm and $c_{Am\text{-}La} = 0.707$ nm; $a_{Nd\text{-}La} = 0.961$ nm and $c_{Nd\text{-}La} = 0.707$ nm) and nearly similar to those of the $Ca_2La_4Nd_4(SiO_4)_6O_2$ ceramic reference ($a_{ceram} = 0.959$ nm and $c_{ceram} = 0.708$ nm) (Table 2).

Table 3 summarizes the residual glass chemical composition of both (Am-La) and (Nd-La) GCs as measured by EPMA. For (Am-La) GC, although close to that of the theoretical "corrected" GC (Table 1), residual glass composition indicates a depletion of Am_2O_3 (1.07 mol. % in comparison to ~1.65 mol.%), La_2O_3 (1.61 mol. % instead of 1.95 mol. %) and CaO (7.30 mol. % in comparison to 8.23 mol. %). The R ratio (R = La/(La + Am)) in the glassy phase is also slightly modified ($R_{residual\ matrix} = 0.60$ instead of R theoretical value of 0.5). For (Nd-La) GC, such phenomena are a bit less marked: the residual glass matrix composition is closer to that of the theoretical (Nd-La) composition in terms of rare earth amounts (Nd_2O_3, La_2O_3), it can only be noticed a lower CaO content (7.62 mol. % instead of 8.20 mol. %) (Table 3).

Apatite phase chemical composition of both (Am-La) and (Nd-La) samples determined by EPMA are reported in Table 4. These results indicate a stoichiometry in lanthanum, neodymium or americium close to that of the theoretical $Ca_2La_4Nd_4(SiO_4)_6O_2$ ceramic phase with a $R_{crystal}$ ratio of 0.5.

Fig. 5-(a) compares Raman spectra of (Am-La) and (Nd-La) residual glass with those of the base glass used as a free-lanthanide-

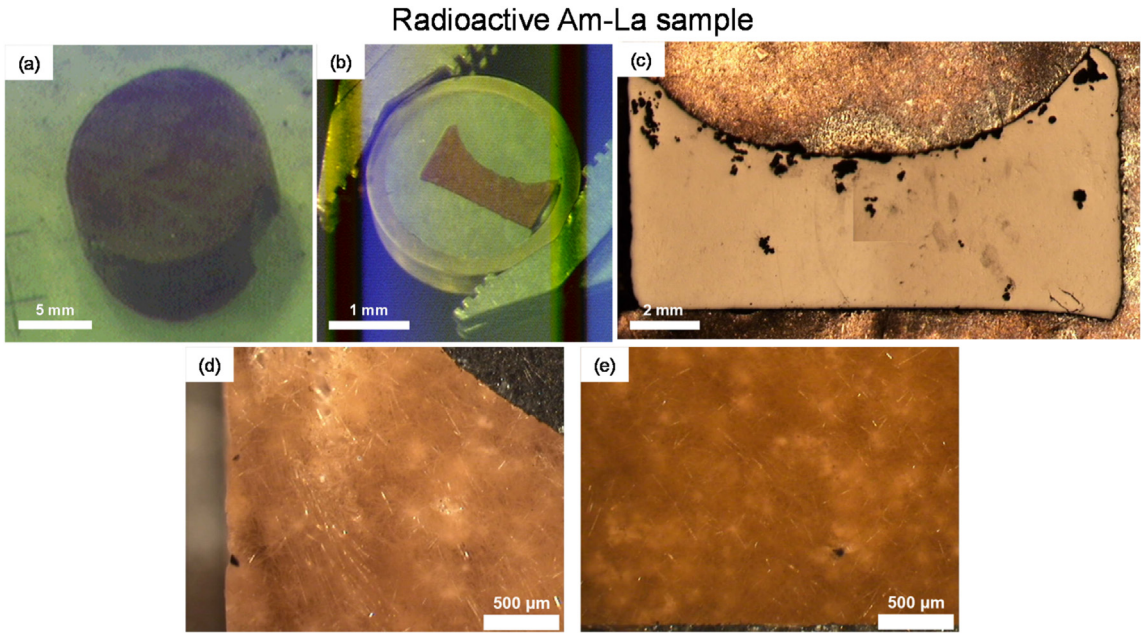

Fig. 1. (Am-La) GC optical microscopy images.

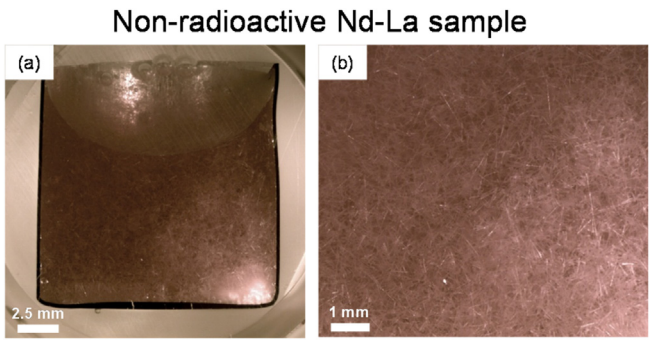

Fig. 2. (Nd-La) GC optical microscopy images.

actinide reference (Table 1) and Table 5 indicates fitted areas of 850–1250 cm^{-1} ranges. This region is attributed to the stretching motion of silicon oxygen bonds in SiO_4 units with Q^n connectivity (where n is the number of bridging oxygen atoms per tetrahedron). This band has been deconvolved into several components, using the second derivative of the signal and data from the literature as shown in Table 5 [23–25].

In the base glass, spectrum deconvolution yields three components at 970, 1070 and 1145 cm^{-1} that could be assigned to Q^2/Q^4(2Al)/Q^4(2B), Q^3(Na + Ca) and Q^4(Al)/Q^4(B) silicate tetrahedra, respectively [23–28]. At lower frequencies two main bands are detected at 505 and 630 cm^{-1} assigned to mixed Si-O-Si bending and rocking mode and to the breathing mode of danburite rings (four members ring containing two silica and two boron tetrahedra), respectively [27,29]. Raman bands between 630 and 800 cm^{-1} are also observed whose origin arise mainly to borate units and to O-Si-O bonds and will not be discussed here, because of overlapping and of a lack of discernable features [10,30,31].

In the (Am-La) and (Nd-La) GCs the main 850 - 1250 cm^{-1} band shifts towards lower wavenumbers compared to the base glass. Deconvolution of the Q^n band needs the introduction of four components instead of three, with the replacement of the band at 970 cm^{-1} by two bands at 933 and 998 cm^{-1}. It is known that the

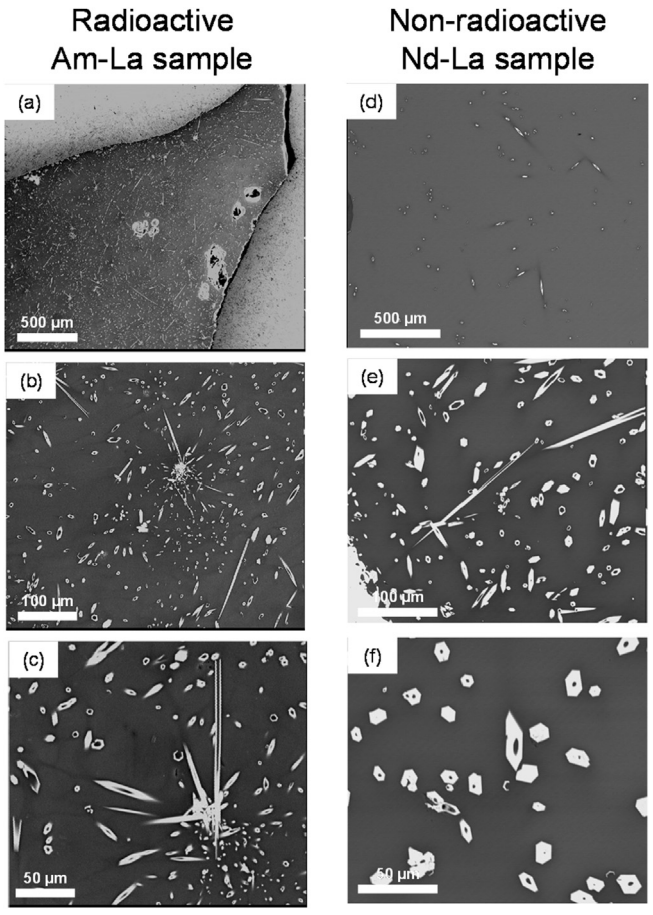

Fig. 3. (a-c) (Am-La) GC and (d-f) (Nd-La) GC SEM micrographs (backscattered electrons). White and dark phases correspond to crystals and residual glass, respectively.

position of a specific band associated to a Qn unit is strongly dependent of the valence state of the neighboring cations. Q^3 band

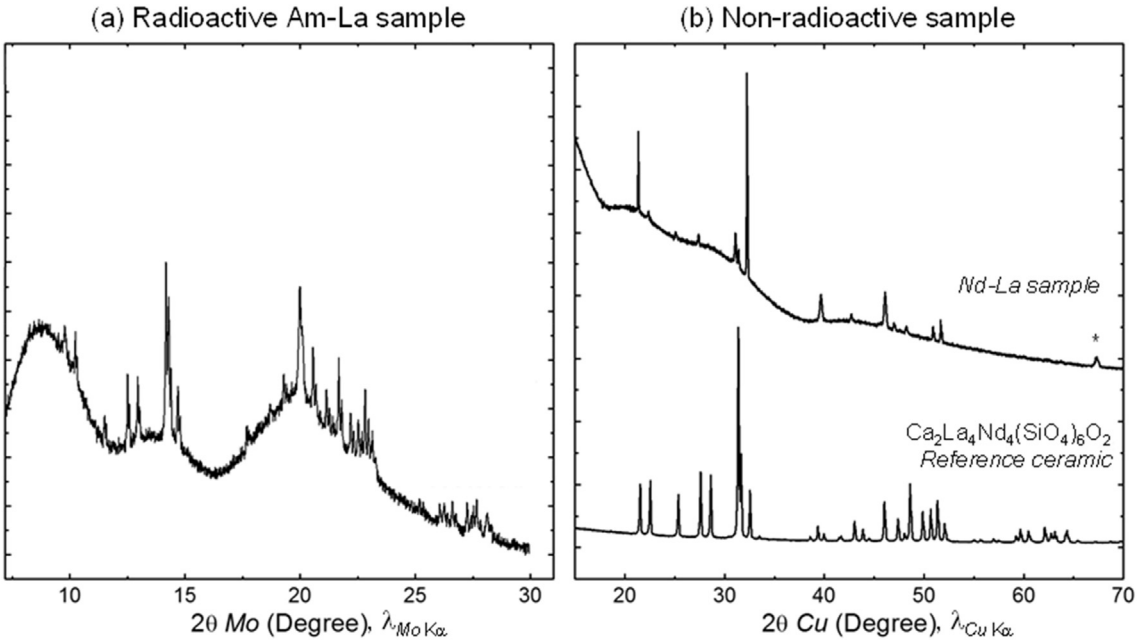

Fig. 4. a) (Am-La) GC and b) (Nd-La) GC and $Ca_2La_4Nd_4(SiO_4)_6O_2$ ceramic reference X-ray diffraction patterns. All the reflections can be assigned to an apatite $Ca_2RE_8(SiO_4)_6O_2$ structure (ICCD card 01-078-1127 ($Ca_2Nd_8(SiO_4)_6O_2$) or 01-071-1368 ($Ca_2La_8(SiO_4)_6O_2$)) except the additional reflection marked (*) due to Pt residues coming from the crucible.

were observed at 1100 cm^{-1} for $Q^3(Na^+)$, [32] at 1060-1080 cm^{-1} for $Q^3(Ca^{2+}, Sr^{2+})$ [28,33,34], at 1010-1040 cm^{-1} for $Q^3(Y^{3+}, La^{3+}, Zr^{4+})$ [34,35]. Therefore, the band at 998 cm^{-1} could be assigned to Q^3 units surrounded by Ln^{3+}/Ac^{3+}, with also a possible contribution from Q^2 tetrahedra [35] exclusively surrounded by Ca^{2+}/Na^+ that is observed at around 950-970 cm^{-1} (Table 5) [33]. Subsequently, the new band at 933 cm^{-1} could be assigned to Q^2 silicate units connected to several lanthanides (Ln^{3+}: La^{3+}, Nd^{3+}) and/or actinide (Ac^{3+}: Am^{3+}) cations.

Table 2
Cell parameters computed from the XRD Patterns of (Am-La) and (Nd-La) glass-ceramics and $Ca_2La_4Nd_4(SiO_4)_6O_2$ ceramic.

Cell parameters	(Am-La)	(Nd-La)	$Ca_2La_4Nd_4(SiO_4)_6O_2$
a (nm)	0,960(2)	0,961(3)	0,959(1)
c (nm)	0,707(1)	0,707(1)	0,708(1)
V (nm^3)	0,564(5)	0,565(6)	0,564(3)

Raman spectra of crystals formed in (Am-La) and (Nd-La) GCs are very similar (Fig. 5-(b)). In both (Am-La) and (Nd-La) crystals, the symmetric stretching mode of SiO_4 (ν_1) appears around 852-854 cm^{-1} and the associated asymmetric stretching motion (ν_3 ~ 920 cm^{-1}) is hidden by contributions from the residual glass matrix. Both symmetric (ν_2) and asymmetric (ν_4) bending modes are found at 394 and 527 cm^{-1}, respectively [31,35]. A slight difference lies in the fact that ν_1 Full Width at Half Maximum (FWHM) value was found to be higher in the (Am- La) crystals than in the (Nd-La) and in the $Ca_2La_4Nd_4(SiO_4)_6O_2$ ceramic (Table 6). This origin could be related to the radiation damage generated by Am alpha decays, even if the characterization were performed rapidly after the elaboration process to minimize this effect.

4. Discussion

Thanks to prior investigations on the solubility limit of Nd_2O_3

Table 3
Electron probe microanalysis of (Am-La) and (Nd-La) residual glass matrix (mol. %).

	Residual glass composition from EPMA (mol. %)								$R_{residual\ matrix}$[a]
	SiO_2	B_2O_3	Na_2O	Al_2O_3	CaO	Am_2O_3	Nd_2O_3	La_2O_3	Matrix
(Am-La) sample	57.21	9.67	18.24	4.90	7.30	1.07	__	1.61	0.60
(Nd-La) sample	57.04	9.27	17.15	5.14	7.62	__	1.86	1.92	0.51

[a] R = La/(La + Am) or La/(La + Nd).

Table 4
Electron probe microanalysis of (Am-La) and (Nd-La) crystalline phases (atomic %). SiO_4 tetrahedra's stoichiometry was fixed at 6 in order to present results according to the stoichiometry $Ca_wLn_xAc_y(SiO_4)_6O_z$.

	Crystals composition from EPMA (atomic %)					$R_{crystal}$[a]
	Ca	La	Nd	Am	O	Crystal
Am-La sample	2.02	3.96	__	4.07	1.99	0.49
Nd-La sample	2.81	3.62	3.57	__	1.59	0.50
Theoretical	2	4	4		2	0.50

[a] R = La/(La + Am) or La/(La + Nd).

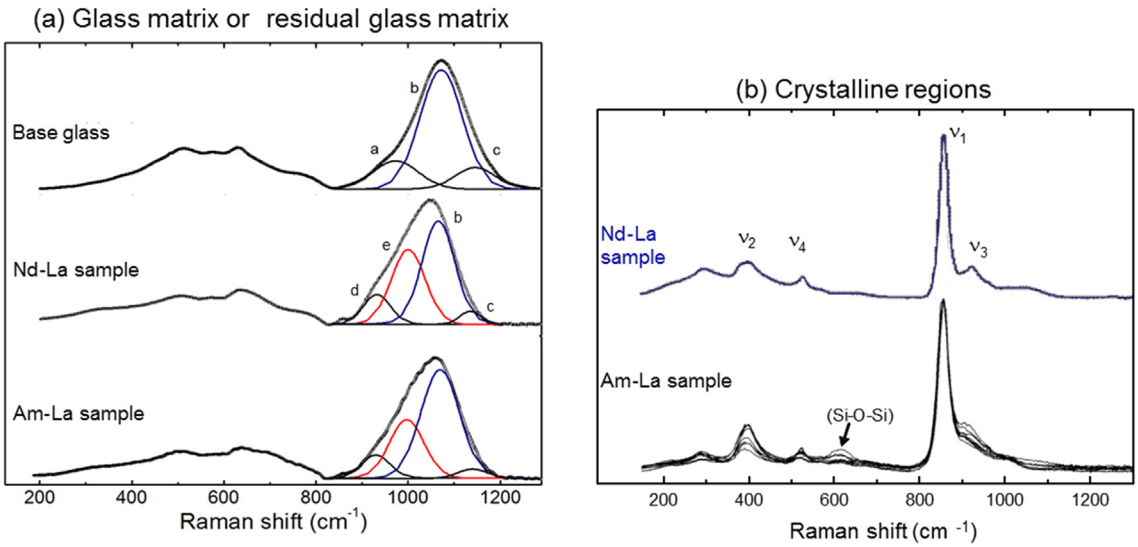

Fig. 5. (a) Raman spectra of base glass (lanthanide-free reference), (Am-La) and (Nd-La) residual glass matrices. Base Glass: a) SiO_4Q^2 (970 cm^{-1}), b) SiO_4 Q^3 (1070 cm^{-1}), c) SiO_4 Q^4 (1148 cm^{-1}), (Am-La) and (Nd-La) residual glass: d) $Q^1/Q^2_{Ln/Ac}$ (933 cm^{-1}), e) $Q^2/Q^3_{Ln/Ac}$ (998 cm^{-1}), b) SiO_4 Q^3 (1070 cm^{-1}), and c) SiO_4 Q^4 (1148 cm^{-1}). (b) Raman spectra of (Am-La) and (Nd-La) crystals.

Table 5
SiO_4 Q^n fitted areas of (Am-La) and (Nd-La) residual glass and base glass Raman spectra.

	Raman shift (cm^{-1})				
	933 $Q^2_{Ln/Ac}$	970 Q^2	998 $Q^3_{Ln/Ac}$[a]	1070 Q^3	1148 Q^4
Base glass	—	17	—	72	11
(Am-La) residual glass	11	—	28	56	5
(Nd-La) residual glass	8	—	36	53	3

[a] Ln: lanthanides, Ac: actinides.

and La_2O_3 in the $SiO_2 - B_2O_3 - Al_2O_3 - Na_2O - CaO - La_2O_3$ - Nd_2O_3 system ((Nd-La) system) [10], a composition of a glass-ceramic in the $SiO_2 - B_2O_3 - Al_2O_3 - Na_2O - CaO - La_2O_3$ - Am_2O_3 system ((Am-La) system) has been determined and tested, relying on a presumed assumption that Nd and Am closely mimic one another in crystal chemistry.

The first notable statement is that the (Am-La) GC contains a homogeneous dispersion of crystals, as theoretically wanted, with an Am_2O_3 content close to the target value.

Comparing (Am-La) GC with its counterpart (Nd-La) - elaborated with the same process —XRD, SEM/EDS, EMPA and Raman characterizations have clearly shown that Am and Nd have similar behavior in both glass-ceramic samples. Indeed, both (Am-La) and (Nd-La) GCs present a similar microstructure and identical crystals morphology, with a dispersion of hexagonal shaped crystals of varying sizes and orientations. In both glass-ceramics, crystals formed in the same apatite-like structure ($P6_3/m$ space group), of general formula $Ca_2La_xAm_{8-x}(SiO_4)_6O_2$ and $Ca_2La_xNd_{8-x}(SiO_4)_6O_2$, respectively. Furthermore, cell parameters of (Am-La) and (Nd-La)-apatite crystals are almost identical and also close to that of the $Ca_2La_4Nd_4(SiO_4)_6O_2$ ceramic reference. Raman data on crystals formed in both (Am-La) and (Nd-La) glass-ceramic materials are also very close. These results are confirmed by EPMA, leading to the determination of very close apatite compositions: $Ca_{2.02}La_{3.96}Am_{4.07}(SiO_4)_6O_{1.99}$ and $Ca_{2.81}La_{3.62}Nd_{3.57}(SiO_4)_6O_{1.59}$, respectively. The values of the R ratios, close to 0.5 in both (Am-La) and (Nd-La) apatite crystals (R = La/(La + Am) or La/(La + Nd)), put forward the fact that the two Nd^{3+} and Am^{3+} behave in a similar manner, i.e. both cations are congruently incorporated in the crystalline phase during the crystallization process. It can be noticed that the Ca content is maybe overestimated in the apatite phase of the (Nd-La)-GC, certainly due to a lower electron acceleration voltage (12 kV instead of 20 kV for (Am-La)-GC analyses).

Within the amorphous glass matrix, Nd^{3+}, La^{3+} and Am^{3+} also behave in a similar manner; the incorporation of both elements to the base glass induces a global shift of the Q^n unit vibration bands toward lower wavenumbers due to the connectivity of both Ln^{3+} and Am^{3+} to the silicon units. This global shift is an indication of a modifier role of both Ln and Am in the glassy network as already demonstrated for Ln [36] with specific ^{17}O NMR experiments and for Am with EXAFS studies showing a similar field strength of around $0.5A^{-2}$ for Ln^{3+} and Ac^{3+} [6].

In the base glass, used as a non-disrupted network reference, most of the sodium atoms are used as charge compensators for alumina and boron tetrahedra. Because NMR analysis of this glass revealed around 61% of boron atoms in fourfold coordination, and because AlO_4 tetrahedra are preferentially compensated by Na atoms, only around 5.1 mol. % of Na_2O are still available for creating NBO atoms. Consequently, NBOs are created either by Ca and to a less extent Na atoms (8.5 mol. % of CaO compared to 5.1 mol. % of Na_2O in a modifier role). It is known that the Si-O stretching vibrations of Q^3(Na) and Q^3(Ca) are located at around 1100 and 1060-

Table 6
Characteristics of the ν_1 Raman motion of crystals formed in (Am-La) and (Nd-La) glass-ceramics and $Ca_2La_4Nd_4(SiO_4)_6O_2$ ceramic reference.

	(Am-La) crystals	(Nd-La) crystals	$Ca_2La_4Nd_4(SiO_4)_6O_2$ ceramic reference
Raman ν_1 position (cm^{-1})	852(1)	854(1)	857(1)
Raman ν_1 FWMH (cm^{-1})	29(2)	23(1)	15(2)

1080 cm^{-1}, respectively. Therefore, the broad band at 1070 cm^{-1} comes certainly from a mixture of these two contributions. The weaker band observed at 1145 cm^{-1} could be attributed to Q^4(Al) and Q^4(B) as generally assigned in aluminosilicate and borosilicate systems [29–31]. The band at 970 cm^{-1} can be assigned to a mixture of Q^2 units and of Q^4(2Al) or Q^4(2B) as discussed in several articles on aluminosilicate and borosilicate glasses [29–31].

As lanthanides and/or actinides were introduced in this system new bands appeared in the silicon tetrahedral region, attributed to Q^2 and Q^3 silicate units connected to one or several lanthanide (Ln^{3+}: La^{3+}, Nd^{3+}) and/or actinide (Ac^{3+}: Am^{3+}) cations. It means that a part of Q^2 and Q^3 units of the base glass are shifted to lower frequency due to the vicinity of an Ln^{3+}/Ac^{3+} in the silica tetrahedra due to the higher field strength. The introduction of either Am or Nd exactly induces the same effect on the Q^n region of the glassy phases of the (Am-La) and (Nd-La) GCs which indicates a similar role of both Am or Nd in the glassy network, and confirming their modifying role. Therefore Nd can be considered as a good surrogate of Am in the glassy network of silicate glasses.

This study, by comparing the incorporation and partitioning of Am and Ln in the two phases of an aluminoborosilicate GC, apatite crystals and glassy phase, have demonstrated a similar behavior of Am^{3+} and Nd^{3+} in both phases and that Nd^{3+} can be used as a good surrogate as Am^{3+} in the two phases and in the GC system.

5. Conclusion

This paper aimed to assess a comparison of Actinides (Am) and Lanthanides (Nd) incorporation in High-Level Waste glass-ceramics in terms of Ln^{3+}/Am^{3+} partitioning into crystals and residual glass, stoichiometry and cell parameters of Ln/Am-crystals and influence of Ln/Am nature on the glassy structure.

As reminded here before, neodymium is usually selected as minor-actinide surrogate in glasses, thanks to their common oxidation state (+III) and ionic radius (0.097 nm and 0.108 nm for Am^{3+} when coordinated to 6 (CN6) and 8 (CN8) oxygen atoms respectively and 0.098 nm (CN6) and 0.111 nm (CN8) for Nd^{3+}) [15,16]. In crystalline structures also, both elements are accommodated in their + III oxidation state [2,17,18].

In the present glass-ceramics prepared in the $SiO_2 - B_2O_3 - Al_2O_3 - Na_2O - CaO - Ln_2O_3/Am_2O_3$ system (with Ln = Nd, La) above the Am_2O_3/Ln_2O_3 solubility limit, Am^{3+} and Nd^{3+} behave in a similar manner. In both (Am-La) and (Nd-La) systems apatite silicate crystals were formed of composition $Ca_2La_xNd_{8-x}(SiO_4)_6O_2$ and $Ca_2La_xAm_{8-x}(SiO_4)_6O_2$, respectively. Shape, composition, Ln/Am stoichiometry and cell parameters of apatite crystals of both (Am-La) and (Nd-La) glass-ceramics are very close. Moreover, both Nd^{3+} and Am^{3+} cations are congruently incorporated in the crystalline phase compared to the glass. In the glassy phase the role of both Am^{3+} and Nd^{3+} are similar with a modifier behavior.

This paper thus shows that Nd^{3+} and Am^{3+} behaviors are very close, either in the glass or in the crystalline structure and demonstrated from a structural basis that Nd can be used as a good surrogate of Am in such aluminoborosilicate GC systems.

Acknowledgement

Financial support for this research has been provided within the framework of CEA/AREVA cooperative agreement.

The experimental data on the radioactive material were obtained in the DHA hot cell laboratory (Atalante facility) and the work of all technicians is gratefully acknowledged.

EPMA measurements were conducted by Sylvie Poissonnet at CEA Saclay, France.

References

[1] W.J. Weber, R.C. Ewing, A. Meldrum, The kinetics of alpha-decay-induced amorphization in zircon and apatite containing weapons-grade plutonium or other actinides, J. Nucl. Mater. 250 (2–3) (1997) 147–155.
[2] O. Terra, N. Dacheux, F. Audubert, R. Podor, Immobilization of tetravalent actinides in phosphate ceramics, J. Nucl. Mater. 352 (1–3) (2006) 224–232.
[3] H.-j Matzke, I.L.F. Ray, B.W. Seatonberry, H. Thiele, C. Trisoglio, C.T. Walker, T.J. White, Incorporation of transuranic elements in titanate nuclear waste ceramics, J. Am. Ceram. Soc. 73 (2) (1990) 370–378.
[4] S. Le Gallet, L. Campayo, E. Courtois, S. Hoffmann, Y. Grin, F. Bernard, F. Bart, Spark plasma sintering of iodine-bearing apatite, J. Nucl. Mater. 400 (3) (2010) 251–256.
[5] L. Campayo, S. Le Gallet, Y. Grin, E. Courtois, F. Bernard, F. Bart, Spark plasma sintering of lead phosphovanadate $Pb_3(VO_4)_{1.6}(PO_4)_{0.4}$, J. Eur. Ceram. Soc. 29 (8) (2009) 1477–1484.
[6] X. Deschanels, S. Peuget, J.N. Cachia, T. Charpentier, Plutonium solubility and self-irradiation effects in borosilicate glass, Prog. Nucl. Energy 49 (8) (2007) 623–634.
[7] C.M. Jantzen, F.P. Glasser, Stabilization of nuclear waste constituents in portland cement, Am. Ceram. Soc. Bull. 58 (4) (1979) 459–466.
[8] C.M. Jantzen, F.P. Glasser, E.E. Lachowski, Radioactive waste-portland cement systems: I, radionuclide distribution, J. Am. Ceram. Soc. 67 (10) (1984) 668–673.
[9] J.-M. Gras, R.D. Quang, H. Masson, T. Lieven, C. Ferry, C. Poinssot, M. Debes, J.-M. Delbecq, Perspectives on the closed fuel cycle – implications for high-level waste matrices, J. Nucl. Mater. 362 (2–3) (2007) 383–394.
[10] A. Kidari, J.-L. Dussossoy, E. Brackx, D. Caurant, M. Magnin, I. Bardez-Giboire, Lanthanum and neodymium solubility in simplified SiO_2-B_2O_3-Na_2O-Al_2O_3-CaO high level waste glass, J. Am. Ceram. Soc. 95 (8) (2012) 2537–2544.
[11] C.W. Ponader, G.E. Brown Jr., Rare earth elements in silicate glassmelt systems: I. Effects of composition on the coordination environments of La, Gd, and Yb, Geochimica Cosmochimica Acta 53 (11) (1989) 2893–2903.
[12] A. Quintas, D. Caurant, O. Majérus, J.L. Dussossoy, T. Charpentier, Effect of changing the rare earth cation type on the structure and crystallisation behaviour of an aluminoborosilicate glass, Phys. Chem. Glasses - Eur. J. Glass Sci. Technol. Part B 49 (4) (2008) 192–197.
[13] D.G. Karraker, Actinide valences in borosilicate glass, J. Am. Ceram. Soc. 65 (1) (1982) 53–55.
[14] P.G. Eller, G.D. Jarvinen, J.D. Purson, R.A. Penneman, R.R. Ryan, F.W. Lytle, R.B. Greegor, Actinide valences in borosilicate glass, Radiochim. Acta 39 (1985) 17–22.
[15] R.G. Haire, N.A. Stump, Fundamental chemistry and materials science of americium in selected immobilization glasses, Mater. Res. Soc. Symposium Proc. 465 (1996) 39–46.
[16] S. Sen, Atomic environment of high-field strength Nd and Al cations as dopants and major components in silicate glasses: a Nd LIII-edge and Al K-edge X-ray absorption spectroscopic study, J. Non-Crystalline Solids 261 (1–3) (2000) 226–236.
[17] J. Ito, Silicate apatites and oxyapatites, Am. Mineralogist 53 (1968) 890–907.
[18] C. Keller, K.H. Walter, Darstellung, gitterkonstanten und chemische eigenschaften einiger ternärer oxide des plutoniums, americiums und curiums vom typ MeIIIXVO4, J. Inorg. Nucl. Chem. 27 (6) (1965) 1253–1260.
[19] R.P. Turcotte, J.W. Wald, F.P. Roberts, J.M. Rusin, W. Lutze, Radiation damage in nuclear waste ceramics, J. Am. Ceram. Soc. 65 (12) (1982) 589–593.
[20] W. Weber, F. P. Roberts, "A review of the current status of radiation effects in solid nuclear waste forms", Scientific Basis for Nuclear Waste Management VI. Proceedings of the Sixth International Symposium, Boston 407-414 (1983).
[21] J. Rodríguez-Carvajal, Recent advances in magnetic structure determination by neutron powder diffraction, Phys. B Condens. Matter 192 (1–2) (1993) 55–69.
[22] D.A. Long, Raman Spectroscopy, McGraw-Hill, New-York, 1977.
[23] B.O. Mysen, F.J. Ryerson, D. Virgo, The structural role of phosphorus in silicate melts, Am. Mineralogist 66 (1981) 106–117.
[24] B.O. Mysen, D. Virgo, C.M. Scarfe, Relations between the anionic structure and viscosity of silicate melts-a Raman spectroscopic study, Am. Mineralogist 65 (1980) 690–710.
[25] N.R. Bimalendu, Spectroscopic analysis of the structure of silicate glasses along the joint $xMAlO_2$-$(1-x)SiO_2$(M = Li, Na, K, Rb, Cs), J. Am. Ceram. Soc. 70 (3) (1987) 183–192.
[26] B.G. Parkinson, D. Holland, M.E. Smith, C. Larson, J. Doerr, M. Affatigato, S.A. Feller, A.P. Howes, C.R. Scales, Quantitative measurement of Q(3) species in silicate and borosilicate glasses using Raman spectroscopy, J. Non-Crystalline Solids 354 (2008) 1936–1942.
[27] S. Peuget, E.A. Maugeri, T. Charpentier, C. Mendoza, M. Moskura, T. Fares, O. Bouty, C. Jégou, Comparison of radiation and quenching rate effects on the structure of a sodium borosilicate glass, J. Non-Crystalline Solids 378 (2013) 201–212.
[28] P.W. McMillan, B. Piriou, A. Navrotsky, A Raman spectroscopic study of glasses along the joins silica-calcium aluminate, silica-sodium aluminate, and silica-potassium aluminate, Geochimica Cosmochimica Acta 46 (1982) 2021–2037.
[29] P.W. McMillan, Structural studies of silicate glasses and melts-applications and limitations of raman spectroscopy, Am. Mineralogist 69 (1984) 622–644.
[30] B.N. Meera, J. Ramakrishna, Raman spectral studies of borate glasses, J. Non-

Crystalline Solids 159 (1–2) (1993) 1–21.
[31] H. Li, Y. Su, L. Li, D.M. Strachan, Raman spectroscopic study of gadolinium(III) in sodium-aluminoborosilicate glasses, J. Non-Crystalline Solids 292 (1–3) (2001) 167–176.
[32] T. Furukawa, K. Fox, W.B. White, J. Chem. Phys. 75 (1981) 3226.
[33] P. McMillan, B. Piriou, R. Couty, A Raman study of pressure-densified vitreous silica, J. Chem. Phys. 81 (1984) 4234–4236.
[34] A.J.G. Ellison, P.C. Hess, Raman study of potassium silicate-glasses containing Rb^{+}, Sr^{2+}, Y^{3+} and Zr^{4+} - implications for cation solution mechanisms in multicomponent liquids, Geochimica Cosmochimica Acta 58 (1994) 1877–1887.
[35] A.J.G. Ellison, P.C. Hess, Vibrational spectra of high-silica glasses of the system K_2O-SiO_2-La_2O_3, J. Non-Crystalline Solids 127 (3) (1991) 247–258.
[36] E. Molières, F. Angeli, P. Jollivet, S. Gin, T. Charpentier, O. Majerus, P. Barboux, D. De Ligny, O. Spalla, Int. J. Appl. Glass Sci. (2013) 1–12.